


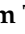




## Article

# Altered Extracellular Vesicle-Derived Protein and microRNA Signatures in Bronchoalveolar Lavage Fluid from Patients with Chronic Obstructive Pulmonary Disease

Sabine Bartel <sup>1,2</sup>, Justina C. Wolters <sup>3</sup> , Hasnat Noor <sup>1,2</sup>, Karim Rafie <sup>4</sup> , Jiahua Fang <sup>1,2</sup>, Benedikt Kirchner <sup>5,6</sup> , Esther Nolte-'t Hoen <sup>7</sup>, Michael W. Pfaffl <sup>5</sup> , Steven Rutgers <sup>8</sup>, Wim Timens <sup>1,2</sup> , Maarten van den Berge <sup>2,9</sup> and Machteld N. Hylkema <sup>1,2,\*</sup> 

- <sup>1</sup> Department of Pathology and Medical Biology, University of Groningen, University Medical Center Groningen, 9713 GZ Groningen, The Netherlands
- <sup>2</sup> Groningen Research Institute for Asthma and COPD (GRIAC), University of Groningen, University Medical Center Groningen, 9713 GZ Groningen, The Netherlands
- <sup>3</sup> Department of Pediatrics, University of Groningen, University Medical Center Groningen, 9713 GZ Groningen, The Netherlands
- <sup>4</sup> Department of Molecular Pharmacology, Groningen Research Institute of Pharmacy (GRIP), University of Groningen, 9712 CP Groningen, The Netherlands
- <sup>5</sup> Division of Animal Physiology and Immunology, School of Life Sciences Weihenstephan, Technical University of Munich, 85354 Freising, Germany
- <sup>6</sup> Institute of Human Genetics, LMU University Hospital, LMU Munich, 80539 Munich, Germany
- <sup>7</sup> Department of Biomolecular Health Sciences, Faculty of Veterinary Medicine, Utrecht University, 3584 CS Utrecht, The Netherlands
- <sup>8</sup> Scheper Hospital, 7824 AA Emmen, The Netherlands
- <sup>9</sup> Department of Pulmonary Diseases, University of Groningen, University Medical Center Groningen, 9713 GZ Groningen, The Netherlands
- \* Correspondence: m.n.hylkema@umcg.nl



**Citation:** Bartel, S.; Wolters, J.C.; Noor, H.; Rafie, K.; Fang, J.; Kirchner, B.; Nolte-'t Hoen, E.; Pfaffl, M.W.; Rutgers, S.; Timens, W.; et al. Altered Extracellular Vesicle-Derived Protein and microRNA Signatures in Bronchoalveolar Lavage Fluid from Patients with Chronic Obstructive Pulmonary Disease. *Cells* **2024**, *13*, 945. <https://doi.org/10.3390/cells13110945>

Academic Editors: Maria Magdalena Barreca and Alexander E. Kalyuzhny

Received: 29 December 2023

Revised: 13 May 2024

Accepted: 24 May 2024

Published: 30 May 2024



**Copyright:** © 2024 by the authors. Licensee MDPI, Basel, Switzerland. This article is an open access article distributed under the terms and conditions of the Creative Commons Attribution (CC BY) license (<https://creativecommons.org/licenses/by/4.0/>).

**Abstract:** Chronic obstructive pulmonary disease (COPD) is a progressive lung disease for which there is no cure. Accumulating research results suggest a role for extracellular vesicles (EVs) in the pathogenesis of COPD. This study aimed to uncover the involvement of EVs and their molecular cargo in the progression of COPD by identification of EV-associated protein and microRNA (miRNA) profiles. We isolated EVs from the bronchial alveolar lavage fluid (BALF) of 18 patients with COPD and 11 healthy controls using size-exclusion chromatography. EV isolates were characterized using nanoparticle tracking analysis and protein content. Proteomic analysis revealed a higher abundance of 284 proteins ( $\log_2FC > 1$ ) and a lower abundance of 3 proteins ( $\log_2FC < -1$ ) in EVs derived from patients with COPD. Ingenuity pathway analysis showed that proteins enriched in COPD-associated EVs trigger inflammatory responses, including neutrophil degranulation. Variances in surface receptors and ligands associated with COPD EVs suggest a preferential interaction with alveolar cells. Small RNAseq analysis identified a higher abundance of ten miRNAs and a lower abundance of one miRNA in EVs from COPD versus controls (Basemean  $> 100$ , FDR  $< 0.05$ ). Our data indicate that the molecular composition of EVs in the BALF of patients with COPD is altered compared to healthy control EVs. Several components in COPD EVs were identified that may perpetuate inflammation and alveolar tissue destruction.

**Keywords:** chronic obstructive pulmonary disease (COPD); extracellular vesicle (EV); proteomics; miRNA; bronchoalveolar lavage (BAL); inflammation

## 1. Introduction

COPD is characterized by persistent airway inflammation, destruction of the extracellular matrix in the lung (emphysema), and chronic mucus hypersecretion, all contributing to irreversible airway obstruction [1]. Current treatments provide symptomatic relief, but

do not address the progression of emphysema. Understanding the molecular mechanisms behind these processes is crucial to develop effective therapies or preventative strategies.

Recent research indicates the involvement of extracellular vesicles (EVs) in various lung diseases. In addition, circulating plasma-derived EVs have been shown to have great potential to be used for the diagnosis, prognosis, and therapeutics of lung diseases such as COPD [2]. EVs, released by virtually all cells in the body, are categorized based on the size and origin into exosomes (<150 nm) derived from multivesicular bodies in endosomes, and microvesicles (~100 nm → 1 µm) shed from the cell surface [3]. EVs functionally transfer various content, including miRNAs, between cells [4]. It is believed that the uptake of EVs is in part regulated by the receptor/ligand interaction with the target cells [5], but relevant receptor/ligand pairs for the interaction of EVs with distinct lung cells are not yet well understood.

Substantial research has linked EVs and their cargo to lung disease (reviewed in [6]), but there are a lack of data regarding their role in COPD. EVs from activated human neutrophils containing neutrophil elastase have been shown to be present in lavage fluid of patients with COPD and to cause tissue destruction resembling emphysema when applied to mice [7]. In contrast, EVs released by mesenchymal stem/stromal cells aid tissue regeneration and dampen inflammation [8], underscoring the varied roles of different EV types in the development and progression of COPD.

Here, we aimed to decipher the distinct molecular signature of EVs in the lungs of patients with COPD. EV-enriched fractions from bronchial alveolar lavage fluid (BALF) were isolated from 11 healthy controls and 18 patients with COPD, and subsequently subjected to untargeted proteomics and small RNA sequencing. Ingenuity pathway analysis (IPA) and a hierarchical clustering analysis of protein abundance revealed that COPD EVs exhibit a different protein and miRNA content, which may enhance the inflammatory responses and degranulation of cells. Specifically, among other proteins, we identified a different presence of surface receptor and ligands on the COPD EVs that could indicate a different cellular origin and an enhanced targeting of alveolar cells of the EVs in COPD compared to controls.

## 2. Materials and Methods

### 2.1. Study Population

All study participants were included in a clinical study performed in the UMCG, as described earlier [9]. Briefly, the study included 11 healthy controls without a history of pulmonary disease and healthy lung function, and 18 patients with moderate COPD (GOLD stage II). All participants were free of asthma and atopy, and all but three non-smoking individuals were ex-smokers with a median of 26.5 pack years (Table 1). Patients were not on medication. Thirteen subjects who had received maintenance treatment with inhaled corticosteroids discontinued this one month prior to the study. Exclusion criteria were treatment with oral corticosteroids and antibiotics or a respiratory tract infection in the month prior to the study. The protocol was approved by the hospital ethics committee. All patients gave their informed consent [9].

### 2.2. Collection and Processing of Bronchoalveolar Lavage

The collection and processing of BALF has been described previously [9]. Briefly, BALF was collected during a bronchoscopy with a flexible fiberoptic bronchoscope (Olympus B1 IT10; Olympus Optical, Tokyo, Japan) in a subsegmental bronchus of the middle lobe. For lavage, four 50 mL aliquots of normal saline pre-warmed to 37 °C were inserted and immediately recovered using a negative pressure of <2.7 kPa (<20 mmHg).

BALF was filtered through a 48 mm nylon gauze (Curapharm249.1 filter; Maxxim Medical Europe, 's-Hertogenbosch, The Netherlands) and recovery and aspect were assessed. After centrifuging for 5 min at 400× g at 4 °C, supernatants were decanted and immediately stored in aliquots at −80 °C.

**Table 1.** Clinical characteristics.

	COPD ( <i>n</i> = 18)	Controls ( <i>n</i> -11)
Age (years)	62 ± 8	58 ± 8
Female/Male	4/14	3/8
Smoking status—ex-smokers (%)	84	100
Pack years	28 ± 22	25 ± 15
FEV <sub>1</sub> (% pred) *	59 ± 13	104 ± 11
FEV <sub>1</sub> /FVC *	66 ± 11	97 ± 8
Bronchoalveolar lavage wash	18	11
Concentration of cells in lavage fluid		
Total cell count per mL	0.061 (0.01–0.6)	0.10 (0.03–0.2)
Macrophages (%)	86 (13.3–94.2)	92 (70.4–96.5)
Neutrophils (%)	1.7 (0.3–85.5)	1.1 (0.1–3.0)
Lymphocytes (%)	6.9 (1.3–26.4)	7.1 (2.5–26.5)
Eosinophils (%)	0.4 (0–1.7)	0.2 (0–0.45)

Data are presented as median (interquartile range), *n*, *n* (%), or mean ± sd, unless otherwise stated. FEV<sub>1</sub>: forced expiratory volume in 1 s; FVC: forced vital capacity. The Mann–Whitney U-test was performed, unless otherwise stated. \*: *p* < 0.05 versus COPD. Table derived from [9].

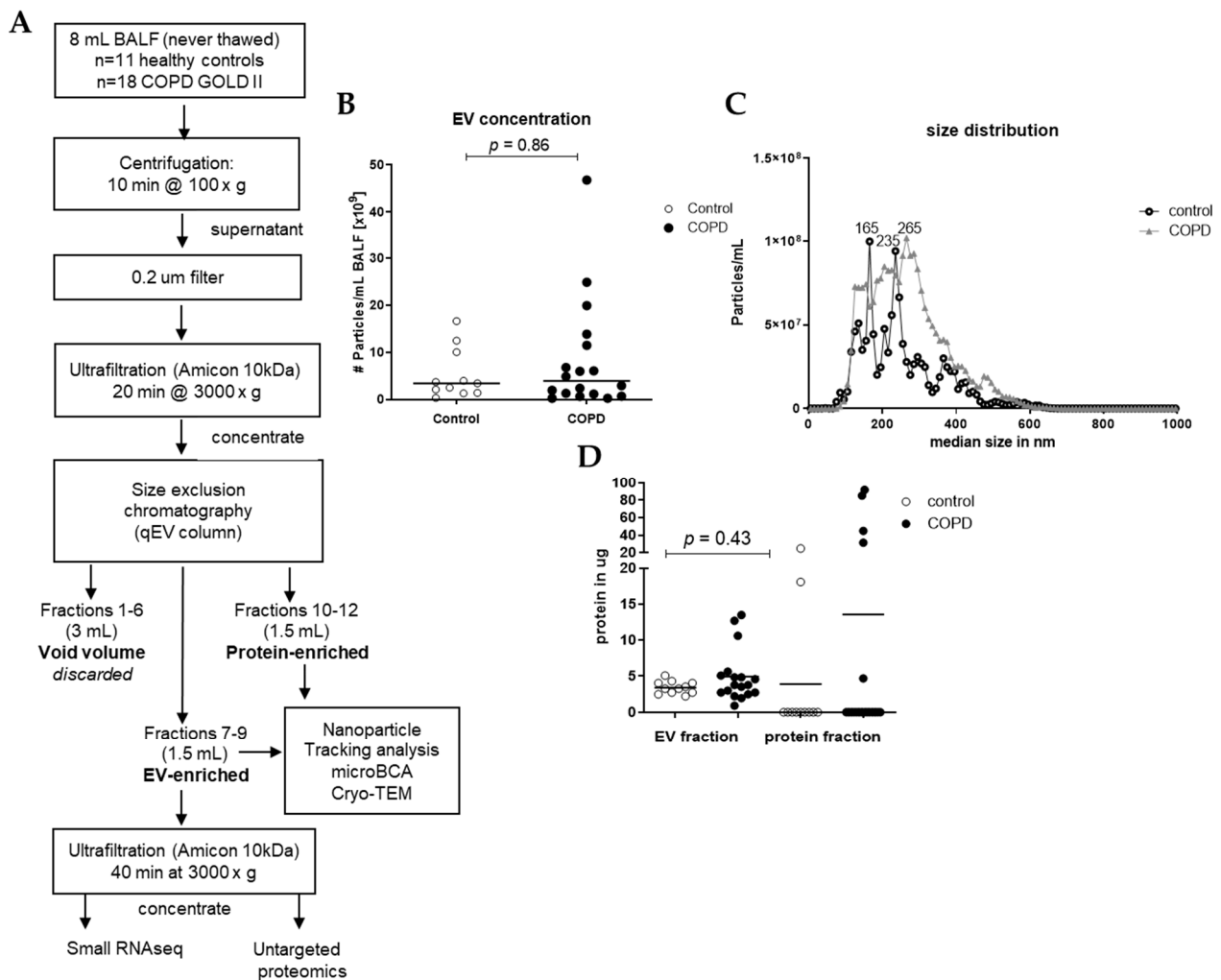
### 2.3. Isolation of EVs from BAL Fluid

EVs were isolated from 8 mL of each sample using different steps of centrifugation, ultrafiltration, and size exclusion chromatography (SEC), as shown in Figure 1. In short, preliminary cellular debris and large vesicles were removed using centrifugation at 1500 × *g* for 10 min (Multifuge X pro Thermo Scientific centrifuge, TX-1000 (7500317)). The BALF was further concentrated and purified using an Amicon filter, filter type 10 kDa (Merck Milipore, Darmstadt, Germany), which was centrifuged at 3000 × *g* for 20 min to concentrate the BALF to 0.5 mL, and this was added to a size SEC qEV original column (35 nm, serial #: 1001659, Izon, Christchurch, New Zealand). Subsequently, 5 × 0.5 mL Hank's Balanced Salt Solution (HBSS, Lonza Bioscience, Walkersville, MD, USA) was added to the column. These 3 mL was referred to as void volume, which was discarded. Consequently, 6 times 0.5 mL HBSS was added to the column, and the first 3 fractions (1.5 mL) were collected in an Eppendorf (EV-enriched fraction) and the last 3 fractions (1.5 mL) were collected in an Eppendorf (protein-enriched fraction). Of the EV-enriched fraction, 1.4 mL was put in an Amicon filter and centrifuged at 3000 × *g* for 40 min to concentrate and purify the EV fraction. After centrifugation, approximately 80 µL was collected and stored at −80 °C until untargeted proteomics, small RNAseq analysis, and Cryo-transmission electron microscopy (Cryo-TEM). The remaining of the EV-enriched fraction and the protein-enriched fraction of the samples were stored at −20 °C until microBCA and nanoparticle tracking analysis (NTA). To assess the concentration of EVs in the isolated SEC fractions, we measured all samples with NTA using a Nanosight camera device (version NTA 3.0 0060, Nanosight, Malvern, UK). The NTA is a powerful technique for characterizing nanoparticles based on their Brownian motion and light-scattering properties, providing valuable insights into the size distribution and concentration of nanoparticles in BALF. All samples were applied to the machine in 1 mL of PBS (1:100 dilution), and three videos of 1 min each were taken and combined for the analysis. The dilution was adjusted individually to achieve between 10–100 particles/frame during the measurement.

### 2.4. Cryo-TEM Imaging

Cryo-TEM was employed to directly visualize vesicle integrity. Initially, a 50 µL EV-enriched sample from a patient with COPD was concentrated to 5 µL using a 500 µL Amicon Ultra Centrifugal filter with a 10 kDa MWCO (Merck, UFC5010BK). Subsequently, a 3 µL aliquot of the concentrated sample was deposited onto glow-discharged holey carbon-coated grids (3.5/1 Quantifoil Micro Tools, Jena, Germany). After the excess liquid was blotted, the grids were vitrified in liquid ethane utilizing a Vitrobot (FEI, Eindhoven, The Netherlands) and then transferred to a FEI Tecnai T20 electron microscope

equipped with a Gatan model 626 cryo-stage operating at 200 keV. Micrographs were captured under low-dose conditions using a slow-scan CCD camera. Images are shown in Supplementary Figure S1.



**Figure 1.** Isolation workflow and characterization of EVs from BALF of healthy controls (n = 11) and patients with COPD (n = 18). (A) Isolation workflow. Isolated EVs were characterized using nanoparticle tracking analysis for the (B) concentration and (C) size and (D) microBCA for protein content. Data are expressed as mean; Mann–Whitney U for COPD vs. control.

### 2.5. Protein Concentration Measurement

Protein measurement was performed with a microBCA kit (ThermoFisher Scientific, Rockford, IL, USA) according to the manufacturer's recommendations. Briefly, 5  $\mu$ L of the isolated EV or protein fractions was diluted with 95  $\mu$ L of PBS in a 96-well microplate and was incubated with BCA reagent for 1 h at 37  $^{\circ}$ C. Each plate contained a standard row of declining BSA concentrations in duplicates (200  $\mu$ g/mL; 50  $\mu$ g/mL; 25  $\mu$ g/mL; 12.5  $\mu$ g/mL, 6.25  $\mu$ g/mL, 3.125  $\mu$ g/mL; 1.56  $\mu$ g/mL and 0  $\mu$ g/mL). Absorbance at 562 nm was assessed using a plate reader (ClarioStart Plus, BMG Labtech, Ortenberg, Germany).

### 2.6. Untargeted Proteomics Analysis

Protein levels were determined using discovery-based proteomics (using label-free quantification) for relative protein concentrations as described previously [10], but with alterations in the LC-MS detection method and subsequent data analyses.

In short, in-gel digestion was performed on 30  $\mu$ L isolated EV material containing an equivalent of the EV isolation from 4 mL of BALF of each sample. Tryptic digestion

(1:100 g/g sequencing grade modified trypsin V5111; Promega, Madison, WI, USA) was performed after reduction with 10 mmol/L dithiothreitol and alkylation with 55 mmol/L iodoacetamide proteins before the peptides were eluted from the gel for mass spectrometric analyses.

Chromatographic separation of the peptides was performed using liquid chromatography (LC) on a nano-HPLC system (Ultimate 3000, Dionex, Sunnyvale, CA, USA) using a nano-LC column (Acclaim PepMapC100 C18, 75  $\mu\text{m}$   $\times$  50 cm, 2  $\mu\text{m}$ , 100  $\text{\AA}$ , Dionex, buffer A: 0.1% *v/v* formic acid, dissolved in milliQ-H<sub>2</sub>O, buffer B: 0.1%, *v/v* formic acid, dissolved in acetonitrile). In general, an equivalent of 60% of the digested starting material from the isolated EVs was injected using the  $\mu\text{L}$ -pickup method with buffer A as a transport liquid from a cooled autosampler (5  $^{\circ}\text{C}$ ) and loaded onto a trap column ( $\mu\text{Pre}$ column cartridge, Acclaim PepMap100 C18, 5  $\mu\text{m}$ , 100  $\text{\AA}$ , 300  $\mu\text{m}$   $\times$  5 mm, Dionex). Peptides were separated on the nano-LC column using a linear gradient from 2–45% buffer B in 117 min at a flowrate of 300 nL/min. The mass spectrometer was operated in positive ion mode and data-independent acquisition mode (DIA) using isolation windows of 12 *m/z* with a precursor mass range of 300–1200. LC-MS raw data were processed with Spectronaut (version 15.1.210713.50606) (Biognosys, Schlieren, Switzerland) using the standard settings of the directDIA workflow, with a human SwissProt database ([www.uniprot.org](http://www.uniprot.org), 20,350 entries, accessed 15 November 2019).

### 2.7. RNA Isolation

After SEC isolation, half of the concentrated EV fraction (30  $\mu\text{L}$ ) was directly added to 700  $\mu\text{L}$  of Qiazol (Qiagen, Venlo, The Netherlands). Isolation of small RNAs was performed with the miRNeasy micro kit (Qiagen) according to the manufacturer's recommendations. RNA was eluted in 14  $\mu\text{L}$  water and stored at  $-80$   $^{\circ}\text{C}$  until the entire sample was subjected to small RNA sequencing.

### 2.8. Small RNA Sequencing

Sequencing of small RNAs, including miRNAs, was performed as previously described using the NEBNext Multiplex Small RNA Library Prep Set for Illumina (New England Biolabs, Ipswich, MA, USA) on a HiSeq 2500 (Illumina, San Diego, CA, USA) with minor modifications to the manufacturer's protocol [11]. In brief, all samples were reduced to a minimal volume using a vacuum centrifuge and were resuspended in 8  $\mu\text{L}$  water. In total, 6  $\mu\text{L}$  thereof was used for NGS library preparation using the NEBNext Multiplex Small RNA Library Prep Set for Illumina (New England Biolabs, Ipswich, MA, USA) with minor modifications to the manufacturer's protocol. Adaptors were ligated to RNA, reverse transcription was performed, and the product was barcoded and amplified using PCR. The size distribution and quantity of resulting cDNA was assessed using a DNA 1000 Kit on a 2100 Bioanalyzer (Agilent Technologies, Santa Clara, CA, USA) before size selection with high-resolution agarose gel electrophoresis. The size range of miRNA-containing cDNA fragments was cut from the gel and purified. After verifying the final library by capillary gel electrophoresis (DNA High Sensitivity Kit, Agilent Technologies), 50 cycles of single-end sequencing were performed on a HiSeq 2500 (Illumina, San Diego, CA, USA).

### 2.9. Statistical Analysis

#### 2.9.1. Proteomics Analysis

For the quantification, the Q-value filtering was set to the classic setting without imputing, which included unpaired *t*-testing for the calculation of the differential abundances between the groups. Raw data with FDR values were exported from the Spectronaut software (version 15.1.210713.50606), and for downstream processing, we only included proteins that were detected in >70% of all samples (20/29). Although a disparity in smoking status between the two groups, due to the small sample size and the predominance of ex-smokers, we did not control for smoking. However, we conducted a correlation analysis on the Foldchange of significant proteins, comparing all samples, with and without the



three non-smoking COPD patients. This analysis demonstrated a high degree of correlation, indicating that the inclusion of non-smoking patients did not significantly impact our findings (see Supplementary Figure S2).

### 2.9.2. Ingenuity Pathway Analysis

Ingenuity pathway analysis (IPA, Qiagen) was performed on proteins and/or miRNAs with a  $\log_2\text{FC} < -1$  or  $>1$  and false discovery rate (FDR)  $< 0.05$  in EVs from COPD patients vs. controls. To this end, we used the IPA function “core analysis”. Selected candidate pathways were chosen according to the level of activation (z-score), significance ( $p < 0.05$ , Fisher’s exact *t*-test), and biological relevance to the research question.

### 2.9.3. Protein Clustering and Functional Annotation

Two-way hierarchical clustering was employed on the top 50 proteins, focusing on their divergence in abundance from control subjects, but independent of both the False Discovery Rate (FDR) and  $\log_2$  fold change ( $\log_2\text{FC}$ ). This method categorized proteins into different groups based on their expression patterns, facilitated by ranking proteins based on their standard deviation, ensuring robustness in the selection process, resulting in the creation of condensed heatmaps. The ComplexHeatmap R/Bioconductor package (Gu 2016) was employed to create heatmaps using scaled  $\log$ -expression values (z-score), applying Euclidean distance and Ward linkage. The standard deviation for ranking and subsequent functional annotation of protein clusters was carried out using the bigOmics analytics tool [12].

To explore the potential involvement in immune pathways, the correlation between protein clusters and functional annotations from immune-related reference sets, available in the Gene Ontology (GO) databases, was examined. The Fisher test for weighting was used to determine the robustness of these correlations.

### 2.9.4. Correlations of Protein Abundance with Macrophage and Neutrophil Cell Number in BALF

Protein abundance from each of the four clusters were correlated with the number of macrophages and neutrophils per 1 mL of BALF of patients with COPD and controls, as well as the lung function parameter FEV1/FVC using Spearman’s test. The quantification of macrophages and neutrophils in BALF was performed using the methods previously described in reference [8].

### 2.9.5. microRNA Expression Profiling

Raw sequencing data were trimmed of tailing adapter sequences with Btrim [13] prior to discarding reads with less than 16 nt in length. To avoid false positive findings, reads mapping to human rRNA, tRNA, snRNA, or snoRNA sequences [14] were filtered from the data set, and remaining reads were directly aligned to mature miRNA sequences obtained from iRbase (v21, [15]) using a Bowtie short read aligner [16]. Differential expression analysis, including the normalization and multiple testing correction using the Benjamini–Hochberg approach, was performed using the DESeq2 package [17] in R [18].

All statistical comparisons (besides the proteomics or miRNAseq analysis) between the two groups were conducted using a Mann–Whitney U test with a threshold of significance of  $p < 0.05$ . All analysis was performed in GraphPad Prism 8.

## 3. Results

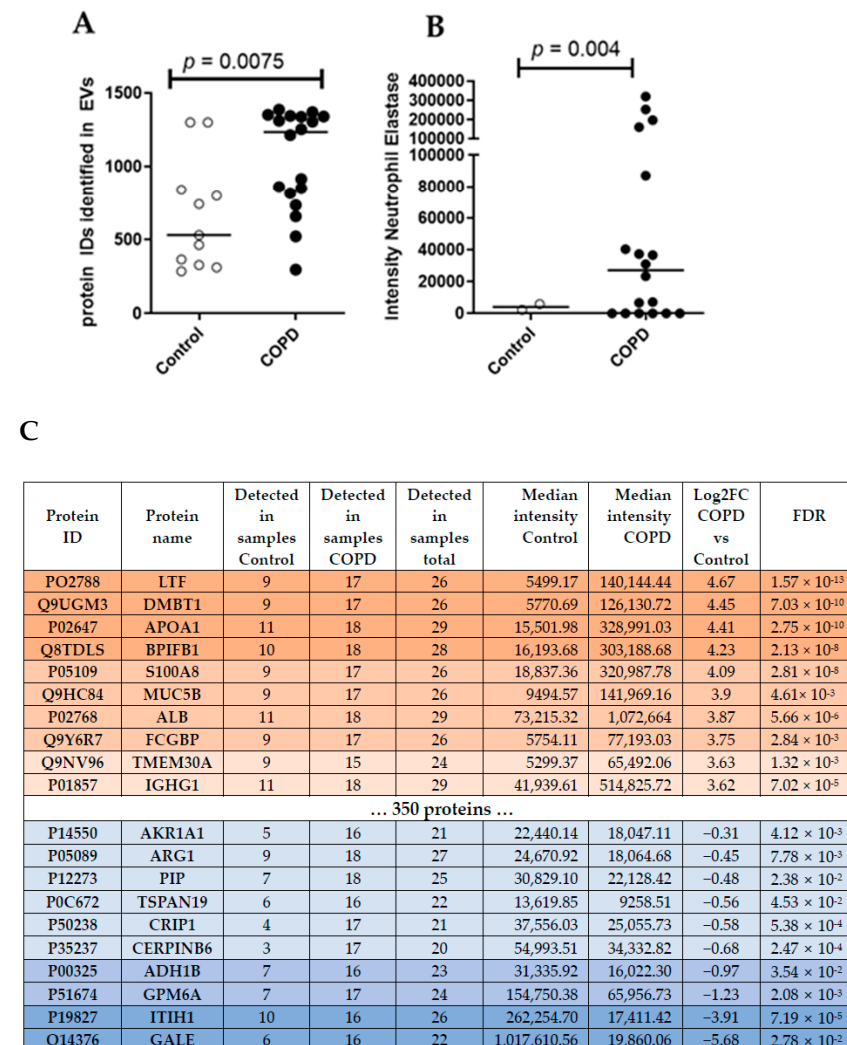
### 3.1. Small EVs Can Successfully Be Isolated from Frozen BALF Samples

Small EVs were isolated from 8 mL of never-thawed BALF aliquots using size exclusion chromatography (SEC) (Figure 1A). Nanoparticle tracking analysis (NTA) of the EV-enriched SEC fractions revealed a median particle count of  $3.42 \times 10^9$  particles/mL for healthy controls and  $3.92 \times 10^9$  particles/mL for COPD samples (Figure 1B). The median size of isolated particles was similar for controls (248 nm) and for COPD BALF

(249 nm) (Figure 1C). Protein quantities were sufficient to proceed to proteomics (Figure 1D). EV-containing fractions were concentrated using ultrafiltration, and equal volumes were subjected to both RNA isolations for small RNA-sequencing and an untargeted proteomics analysis (Figure 1A). Cryo-TEM images of isolated EVs showed that EVs were intact and had a round shape (Figure S1).

### 3.2. Proteomics Analysis of BALF EVs

Unbiased proteomics analysis using LC/MS identified more unique peptides in BALF EVs derived from patients with COPD (median = 1234) compared to healthy controls (median = 531) (Figure 2A). According to the guidelines for minimal information essential for studies of EVs (MISEV) [19], several protein markers need to be present and/or absent from the isolated EVs to judge their integrity and purity. Table 2 lists all markers of the MISEV2018 guidelines and their detection intensity in our samples. Accordingly, we were able to detect the majority of proteins that are frequently found to be present in EVs (i.e., category 1 and 2, Table 2), suggesting that we indeed enriched EVs from our BALF samples. We also detected a contamination with lipoproteins (category 3a, Table 2), as expected by a purely SEC-based isolation [20]. Interestingly, the intensity of most EV-specific markers (Table 2) was higher in COPD samples, indicating a clear enrichment of BALF EVs in COPD.



**Figure 2.** (A) Number of unique peptides identified using LC/MS untargeted proteomics analysis. Mann–Whitney U vs. control. (B) Intensity of Neutrophil Elastase in BALF EVs. (C) Top ten differentially abundant proteins in COPD subjects.

Table 2. Assessment of MISEV EV markers.

MISEV Category	Protein	Detected in Control Samples (Median Intensity)	Detected in COPD Samples (Median Intensity)
<i>1—transmembrane or GPI-anchored proteins</i>			
1a—non-tissue specific	CD63	11/11 (15,509.93)	18/18 (92,003.89)
	CD81	11/11 (94,397.15)	18/18 (126,942.64)
	CD82	10/11 (13,925.97)	18/18 (45,828.48)
	CD47	8/11 (30,198.34)	17/18 (128,907.36)
	GNA	0/11	0/18
	HLA-A	9/11 (23,105.60)	15/18 (66,913.24)
	H2-K/D/Q	0/11	0/18
	ITGA3	3/11 (16,334.62)	15/18 (17,816.25)
	ITGB2	5/11 (28,874.69)	16/18 (43,729.40)
	TFR2	0/11	0/18
	LAMP1	3/11 (31,599.47)	15/18 (28,388.38)
	SDC	0/11	0/18
	BSG	0/11	0/18
	ADAM10	4/11 (24,082.33)	14/18 (47,027.64)
	CD73	0/11	0/18
	CD55	11/11 (29,733.75)	18/18 (162,760.10)
	CD59	11/11 (109,809.55)	18/18 (363,903.25)
1b—tissue specific	CD9	11/11 (185,367.57)	18/18 (612,304.21)
	EPCAM	5/11 (9394.25)	11/18 (9267.61)
	TSPAN8	8/11 (13,506.14)	17/18 (27,948.92)
	CD14	3/11 (18,100.96)	14/18 (20,410.54)
<i>2—cytosolic proteins recovered in EVs</i>			
2a—lipid or membrane-binding ability	ESCRT-I/II/III	0/11	0/18
	TSG101	11/11 (30,495.01)	18/18 (68,322.18)
	ALIX (PDCD6IP)	11/11 (26,746.72)	18/18 (134,175.34)
	ARRDC1	8/11 (22,419.05)	17/18 (114,076.60)
	FLOT1	7/11 (10,344.42)	16/18 (35,016.16)
	CAV	0/11	0/18
	ANXA1	11/11 (49,761.63)	18/18 (406,865.34)
	HSC70	0/11	0/18
	HSP84	0/11	0/18
	ARF6	2/11 (45,850.05)	13/18 (38,333.01)
	SDCBP	11/11 (49,047.33)	18/18 (322,430.85)
	MAPT	0/11	0/18
2b—promiscuous incorporation into EVs	HSP70	0/11	0/18
	ACT	0/11	0/18
	TUB	0/11	0/18
	GAPDH	11/11 (26,518.46)	18/18 (87,466.69)
<i>3—major components of non-EV co-isolated structures</i>			
3a—lipoproteins	APOA1	11/11 (15,501.97)	18/18 (328,991.03)
	APOB	8/11 (81,382.46)	17/18 (19,999.87)
	APOB100	0/11	0/18
	ALB	11/11 (73,215.32)	18/18 (1,072,664.00)
3b—protein–protein/nucleic acid aggregates	UMOD	0/11	0/18
<i>4—Transmembrane, lipid-bound soluble proteins associated with other intracellular compartments than PM/endosomes</i>			
4a—nucleus	HIST1HC	5/11 (16,701.19)	13/18 (27,412.26)
	LMNA	4/11 (9030.91)	14/18 (21,075.30)



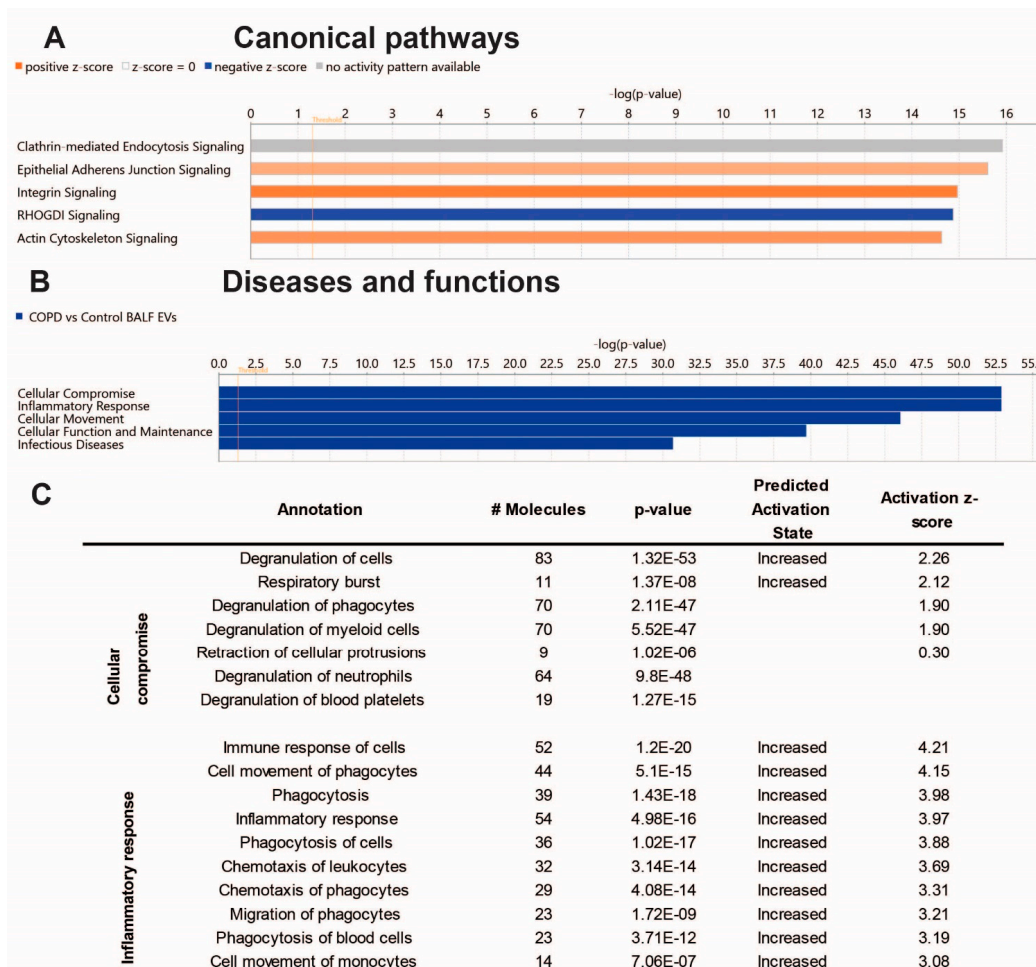
Table 2. Cont.

MISEV Category	Protein	Detected in Control Samples (Median Intensity)	Detected in COPD Samples (Median Intensity)
4b—mitochondria	IMMT	0/11	0/18
	CYC1	0/11	0/18
	TOMM20	0/11	0/18
4c—secretory pathway (endoplasmatic reticulum, Golgi apparatus)	CANX	4/11 (1663.54)	6/18 (16,269.11)
	HSP90B1	3/11 (3891.60)	8/18 (8363.01)
	BIP	0/11	0/18
	GM130	0/11	0/18
4d—autophagosome, cytoskeleton	ATG9A	0/11	0/18
	ACTN1	6/11 (14,611.46)	17/18 (42,763.41)
	KRT18	0/11	0/18
5—Secreted proteins recovered with EVs			
5a—cytokines and growth factors	TGFB1/2	0/11	0/18
	IFNG	0/11	0/18
	VEGFA	0/11	0/18
	FGF1/2	0/11	0/18
	PDGF	0/11	0/18
	EGF	0/11	0/18
	IL	0/11	0/18
5b—adhesion and extracellular matrix proteins	FN1	4/11 (27,088.45)	16/18 (19,794.65)
	COL12A1	0/11	9/18 (12,138.44)
	MFGE8	0/11	0/18
	LGAL3BP	0/11	0/18
	CD5L	6/11 (10,115.46)	16/18 (16,718.95)
AHSG	5/11 (17,509.83)	16/18 (27,092.54)	

To compare different EV-associated protein signatures between COPD and control samples, we focused on the 596 proteins that were detected in at least 70% of all samples (20/29). This approach identified 370 proteins that were significantly (FDR < 0.05) altered in COPD-derived BALF EVs. Thereby, three proteins were down-regulated in COPD EVs compared to controls ( $\log_2FC < -1$ ) and 284 proteins were up-regulated ( $\log_2FC > 1$ ) (Top10 listed in Figure 2C, see Table S1 in the online supplement for the complete list). The top three up-regulated proteins in COPD BALF EVs were Lactotransferrin (LTF,  $\log_2FC = 4.67$ , FDR =  $1.57 \times 10^{-13}$ ), Deleted In Malignant Brain Tumors 1 (DMBT1,  $\log_2FC = 4.45$ , FDR =  $7.03 \times 10^{-6}$ ), and Apolipoprotein A1 (APOA1,  $\log_2FC = 4.41$ , FDR =  $2.75 \times 10^{-10}$ ). UDP-Glucose-4-Epimerase (GALE,  $\log_2FC = -5.68$ , FDR =  $2.78 \times 10^{-2}$ ), Inter-Alpha-Trypsin Inhibitor Heavy Chain 1 (ITIH1,  $\log_2FC = -3.91$ , FDR =  $7.19 \times 10^{-5}$ ), and Glycoprotein M6A (GPM6A,  $\log_2FC = -1.23$ , FDR =  $2.08 \times 10^{-3}$ ) were the top three down-regulated proteins in COPD BALF EVs. We also detected the previously described protein Neutrophil Elastase, important in emphysema development, in all samples of COPD patients, but only in few controls (Figure 2B).

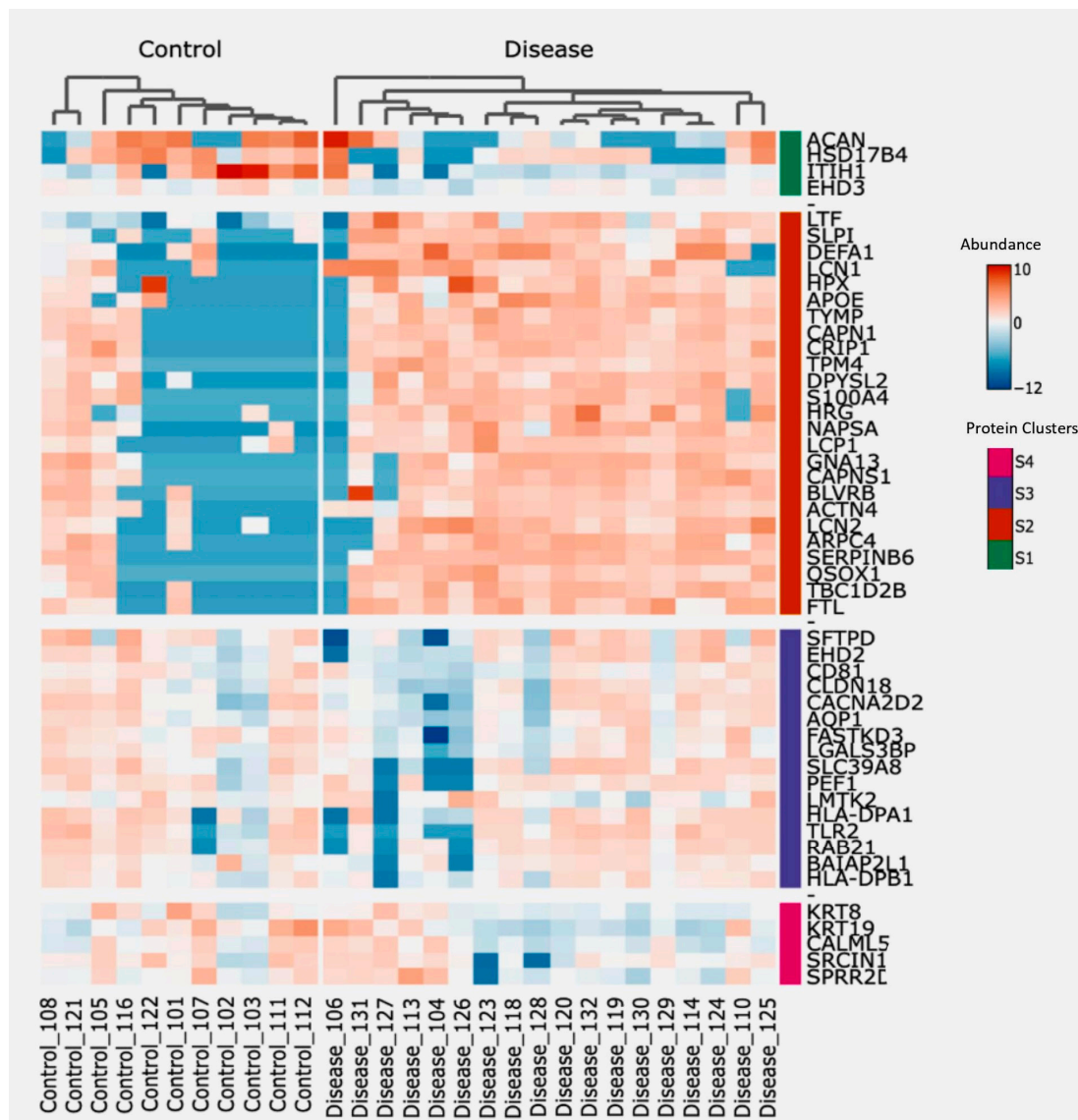
To gain insight into the biological effects of the altered protein content of COPD EVs, we performed Ingenuity Pathway Analysis (IPA). As shown in Figure 3A, IPA analysis revealed proteins associated with COPD-derived BALF EVs most significantly involved in the canonical pathways clathrin-mediated endocytosis signaling, epithelial adherens junction signaling, and integrin signaling. The latter two were predicted to be higher in COPD EVs, while Rho GDP-dissociation inhibitor (RHOGDI) signaling was predicted to be lower in COPD EVs compared to healthy controls. The IPA annotation 'diseases and functions' showed that the protein content of COPD BALF EVs is associated with cellular compromise, inflammatory response, and cellular movement (Figure 3B). Subsections of these annotations are listed in Figure 3C and show that IPA predicts the activation of, for

example, the degranulation and immune response of cells, indicating that EVs in the lung might be functionally involved in COPD pathogenesis.



**Figure 3.** Ingenuity pathway analysis of the BALF EV proteome Core analysis using Ingenuity Pathway Analysis (Qiagen). (A) Subsection ‘Canonical Pathways’ (cut-off  $-\log_{10}, p\text{-value} > 14$ ); (B) subsection ‘Diseases & Functions’ (cut-off  $-\log_{10}, p\text{-value} > 30$ ), and the Table showing associated annotations of the top two functions ‘cellular compromise’ and ‘inflammatory response’ with activity predictions. (C) Image derived from ‘regulator effects’ prediction.

To identify proteins potentially associated with the destructive-immune response in COPD, we conducted a two-way hierarchical clustering analysis focusing on the top 50 proteins ranked by a standard deviation metric. This analysis generated a clustered heatmap displaying protein abundance, with annotated protein groups categorized into four distinct clusters based on their functionalities (Figure 4). Next, we cross-referenced the significantly differentially abundant proteins from our dataset with immune-related datasets to identify correlations (Table 3), showing that the second and third cluster proteins contain the main clusters with a positive correlation to immune-related responses, whereas cluster 4 proteins were negatively correlated to one of the immune-related pathways. Additionally, proteins from each of the four clusters were correlated with both the count of macrophages and neutrophils per mL of BALF from the identical samples used for EV isolation, as well as the lung function parameter FEV1/FVC.



**Figure 4.** Heatmap showing protein abundance of the top 50 proteins, sorted using two-way hierarchical clustering. Red corresponds to the higher and blue corresponds to the lower abundance of the protein. Based on abundance, protein groups are divided into four clusters; S1 (Green), S2 (Orange), S3 (Purple), and S4 (Pink).

**Table 3.** Correlation of the four clusters identified in Figure 4 with immune-related pathways based on a Fisher testing correlation analysis.

Annotations	S1	S2	S3	S4
GO_POSITIVE_REGULATION_OF_IMMUNE_SYSTEM_PROCESS	0	0.44	0.36	0
GO_REGULATION_OF_IMMUNE_RESPONSE	0	0.41	0.37	0
Innate Immune System_Homo sapiens_R-HSA-168249	0	0.34	0.17	0
GO_INNATE_IMMUNE_RESPONSE	0	0.53	0.31	0
GO_POSITIVE_REGULATION_OF_IMMUNE_RESPONSE	0	0.43	0.32	0
GO_IMMUNE_EFFECTOR_PROCESS	0	0.51	0	0
neutrophil activation involved in immune response (GO_000228)	0	0.53	0.62	-0.27
GO_ACTIVATION_OF_IMMUNE_RESPONSE	0	0.23	0.36	0

Table 3. Cont.

Annotations	S1	S2	S3	S4
GO_REGULATION_OF_IMMUNE_EFFECTOR_PROCESS	0	0.30	0	0
GO_NEGATIVE_REGULATION_OF_IMMUNE_SYSTEM_PROCESS	0	0.34	0.34	0
GO_REGULATION_OF_INNATE_IMMUNE_RESPONSE	0	0.48	0.24	0
GO_ADAPTIVE_IMMUNE_RESPONSE	0	0	0	0
GO_POSITIVE_REGULATION_OF_INNATE_IMMUNE_RESPONSE	0	0.43	0.29	0
Hepatitis, Autoimmune C0241910 mouse GSE867 sample 230 (down)	0	0.56	0	0
GO_ACTIVATION_OF_INNATE_IMMUNE_RESPONSE	0	0	0.35	0
GO_HUMORAL_IMMUNE_RESPONSE	0	0.67	0	0
innate immune response activating cell surface receptor signaling pathway.	0	0	0	0

The results presented in Table 4 reveal significant correlations between the abundance of specific proteins with macrophage and neutrophil numbers in BALF. In controls, both lectin galactoside-binding soluble 3-binding protein (LGALS3BP) and BAIAP2L1 encoding insulin-responsive protein of mass 53 kD (IRSp53) correlated negatively with BALF macrophage numbers ( $r = -0.60$ ,  $p = 0.03$  and  $r = -0.67$ ,  $p = 0.02$ , respectively). Conversely, in COPD EVs, Apolipoprotein E (APOE) exhibited a negative correlation with macrophage numbers ( $r = -0.49$ ,  $p = 0.04$ ), while Aquaporin1 (AQP1) showed a positive correlation ( $r = 0.51$ ,  $p = 0.03$ ) with macrophage numbers. Notably, the abundance of proteins from these four clusters did not display significant correlations with neutrophil numbers in BALF from the same individuals.

Table 4. Correlation of protein groups with FEV1/FVC and number of macrophages and neutrophils in BALF.

Parameter	Protein	Correlation	<i>p</i> -Value
<b>Lung function</b>			
Controls	LCN2	0.60	0.03
COPD	APOE	-0.45	0.05
	LTF	-0.50	0.04
<b>Macrophages in BALF</b>			
Controls	LGALS3BP	-0.60	0.03
	BAIAP2L1	-0.67	0.02
COPD	APOE	-0.49	0.04
	AQP1	0.51	0.03
<b>Neutrophils in BALF</b>			
Controls	-	-	-
COPD	-	-	-

In relation to lung function, noteworthy correlations emerged between specific proteins in EVs and the FEV1/FVC parameter. In control EVs, abundance of Lipocalin-2 (LCN2) correlated positively to FEV1/FVC ( $r = 0.60$ ,  $p = 0.03$ ), whereas abundance of Apolipoprotein E (APOE) and the neutrophil granule protein Lactoferrin (LTF) correlated negatively to FEV1/FVC ( $r = -0.45$ ,  $p = 0.05$  and  $r = -0.50$ ,  $p = 0.04$ , respectively) in COPD EVs.

### 3.3. Altered Receptor/Ligand Pattern on BALF EVs in COPD

Identification of receptors on EVs can potentially be used to delineate the cells of EV origin, while characterization of ligands may identify target cell types with which EVs can interact. We screened the proteins detected in >70% of samples of each group for all identified human receptors and ligands (derived from CellTalkDB [21]). Of the 35 identified receptors, 11 were found on COPD EVs but not in controls (Figure 5A, Table S2 of online supplement). Our BALF EV dataset contained 96 ligands, of which 51 ligands were enriched in COPD EVs (Figure 5B, Table S3 in online supplement). By using the EV analysis tool Funrich [22], we were able to associate the receptors on our BALF EVs to their cellular origin. Figure 5C shows that BALF EVs derived from COPD patients seem to be derived relatively more from immune cells, such as neutrophils, eosinophils, or macrophages. To identify the potential target cells, we listed the respective receptors that are paired to the ligands on the BALF EVs (Figure 5D) and the number of ligands in our dataset that are able to interact with these receptors according to CellTalkDB [21]. Accordingly, the receptors for which ligands are present on control BALF EVs from healthy individuals are Integrin beta 2 (ITGB2, 8 interactions), LDL receptor-related protein 1 (LRP1, 7 interactions), and Toll-like receptor 4 (TLR4, 7 interactions). COPD BALF EVs are enriched in ligands that can interact with LRP1 (12 interactions), LRP2 (12 interactions), and epidermal growth factor receptor (EGFR, 11 interactions) (Figure 5D).

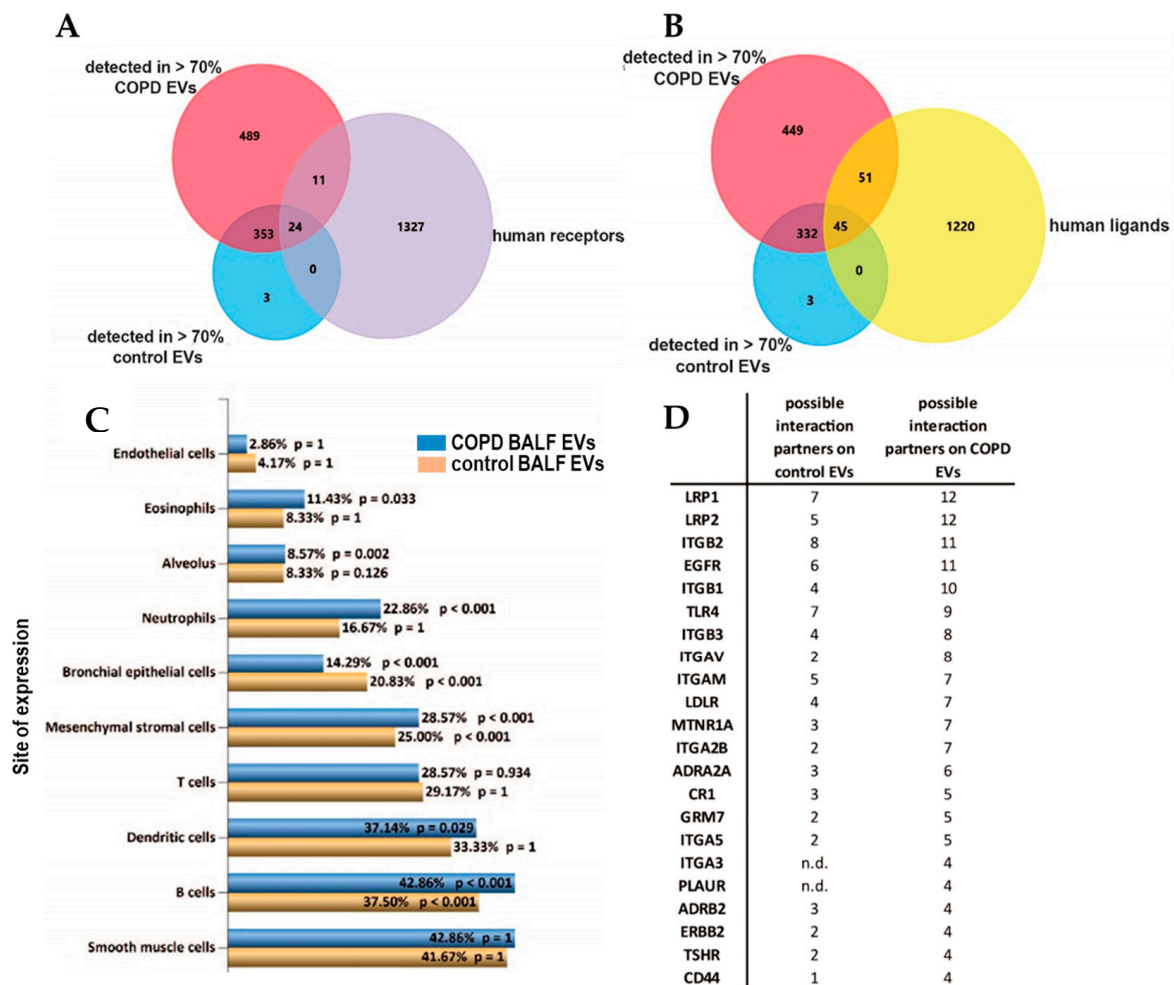
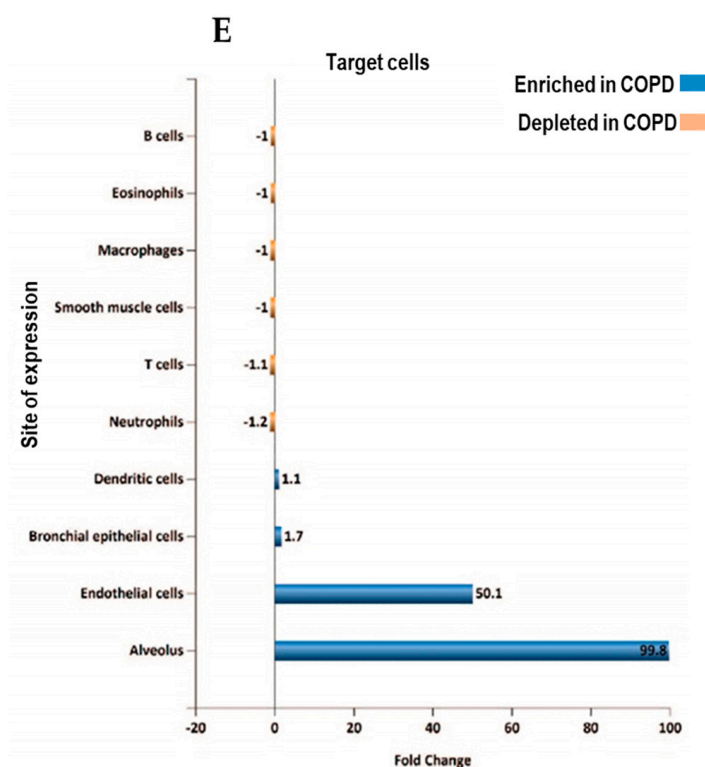


Figure 5. Cont.





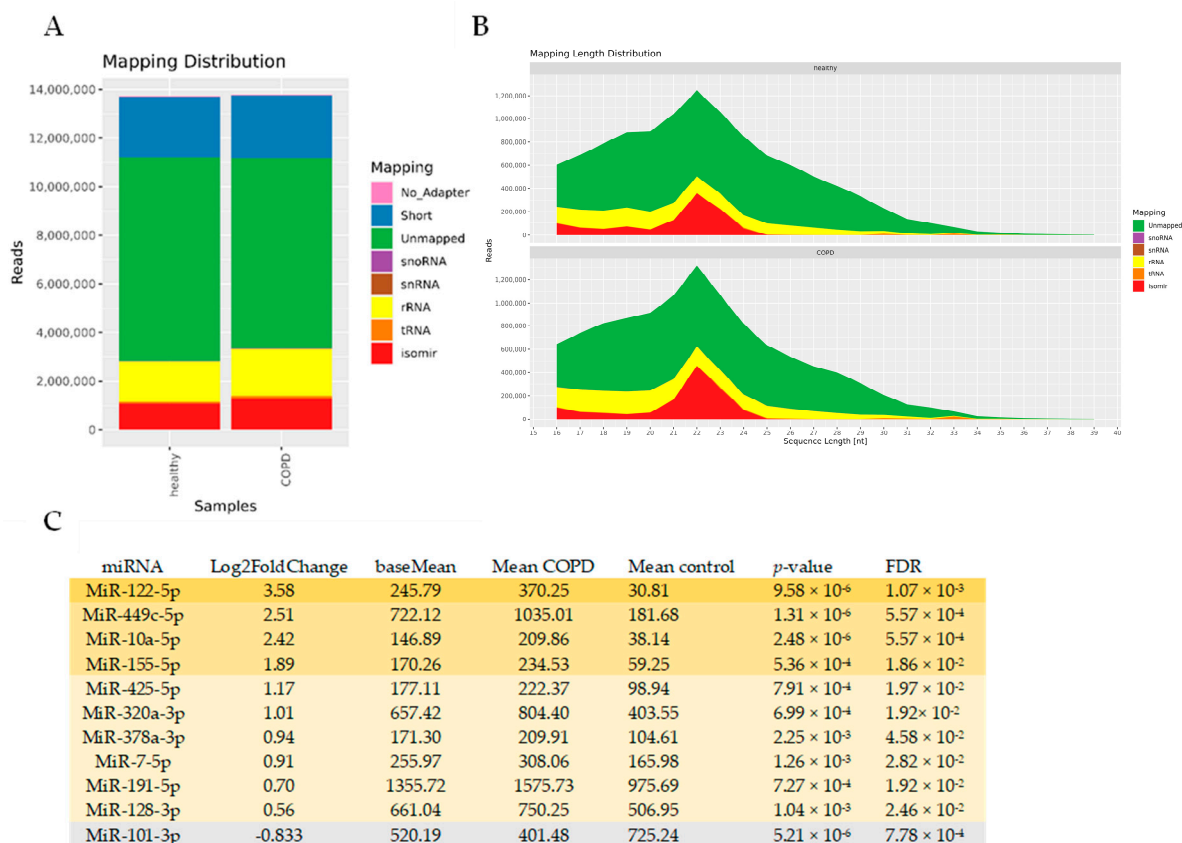
**Figure 5.** Altered receptor/ligand patterns on the EV surface of BALF EVs in COPD. (A) Venn Diagrams to determine the expression of receptors (purple) and (B) ligands (yellow) derived from CellTalkDB (yellow) on EVs from both COPD (red) or healthy control EVs (blue). (C) Cellular origin of EVs predicted using the detected receptors on all BALF EVs (yellow), and receptors detected on COPD EVs (blue) using FUNRICH ‘site of expression’ analysis. (D) List of cellular receptors and amount of ligands on BALF EVs that are possible interaction partners. (E) FUNRICH site of expression analysis of the cellular receptors addressed by control or COPD BALF EVs.

A Funrich site of expression analysis revealed an almost 100-fold enrichment of interactions between the EVs in COPD and the alveolus (Figure 5E), and interactions with endothelial cells were predicted to be enriched 50-fold.

### 3.4. miRNAseq Analysis of BALF EVs

To identify miRNAs associated with EVs in COPD, we performed an unbiased RNA-seq analysis of isolated BALF EVs. In general, sequencing was successful in all 29 samples, with high quality scores. The mapping distribution revealed a relatively small yet expected percentage of miRNAs in the sequencing reads (~10%), which still reached 1 million reads (Figure 6A,B) and a large percentage of unmapped reads (which might include truncated RNAs). Of the 1400 detected miRNAs, 96 miRNAs had a base mean expression value of >100, ensuring sufficient expression across both COPD and control EVs (see Supplementary Table S4 for the full list). Eleven miRNAs showed differential abundance between COPD and controls with an FDR < 0.05 (Figure 6C). Ten miRNAs showed higher abundance (miR-122-5p, miR-449c-5p, miR-10a-5p, miR-155-5p, miR-425-5p, miR-320a-3p, miR-378a-3p, miR-7-5p, miR-191-5p, and miR-128-3p), whereas one miRNA was detected in lower abundance (miR-101-3p) compared to healthy controls (Figure 6C). Due to the low number of differentially abundant miRNAs, we did not perform an IPA analysis. Abundance of miRNAs was also not correlated with immune cell numbers and lung function.





**Figure 6.** Altered miRNA expression in BALF-derived EVs of COPD patients compared to healthy controls. (A) Mapping distribution of small RNA-sequencing expressed in read counts (B) and length. (C) Table with ten up- and one down-regulated miRNAs with a base mean of >100 and FDR < 0.05.

#### 4. Discussion

This is the first study to investigate both the protein and small RNA content of EVs derived from BALF samples of patients with COPD and healthy controls. We identified 284 up- and 3 down-regulated proteins in COPD BALF EVs compared to healthy controls, and 10 up-regulated and one down-regulated miRNA. Our data suggest that the protein signature found in pulmonary EVs in COPD sustains inflammatory reactions and cellular dysfunction. Analyzing the receptor and ligand patterns on the EVs provided suggestive evidence that EVs in COPD originated from immune cells rather than structural cells, and that their potential target cells reside in the alveolar region. The suggestion of immune cell-derived COPD EVs was supported by the correlations between protein abundance and macrophage numbers in the corresponding BALF samples. Consequently, the altered composition in EVs in the BALF reflects the predominant feature of COPD, which is persistent inflammation, resulting potentially in an imbalance between tissue damage and repair in the alveolar target cells.

The most prominently up-regulated protein in COPD EVs was Lactotransferrin. LTF is known as an antimicrobial peptide released from goblet cells in the airway epithelium or from glands [23]. While LTF is a component of the airway lining fluid, it has also been reported to be present in BALF and increased in chronic bronchitis [23,24]. Although there has not been any prior association reported between LTF and EVs in the lung, recent discoveries have highlighted its presence, along with other antimicrobial peptides, in EVs secreted by human mesenchymal stem/stromal cells [25]. Additionally, studies have indicated its increased presence in EVs released from primary human neutrophils following in vitro stimulation [7]. Notably, in our study, we did not find a correlation with LTF

abundance and the number of neutrophils in BALF. This suggests that LTF could be secreted by different cell types in COPD.

DMBT1, found to be up-regulated in COPD BALF EVs, belongs to the category of innate defense proteins. This protein has been described to be increased in an alveolar cell line following hypoxic conditions, where it plays a role in surfactant function [26]. Moreover, it has demonstrated the ability to stimulate repair mechanisms in alveolar cells by reducing IL-6 levels while enhancing vascular endothelial growth factor (VEGF) production [27]. Beyond its intracellular function, DMBT1 has been identified in human stem cell-derived EVs, which exhibit similar angiogenic properties and facilitate a repair-inducing effect [28]. These collective findings suggest that DMBT1 might contribute to repair and angiogenic mechanisms in the lung, potentially influencing repair mechanisms and surfactant modulation in the context of COPD.

The third most prominently up-regulated EV-associated protein in COPD, ApoA1, raises some intriguing possibilities. It has been considered to be a potential contaminant from lipoproteins during EV isolation, but may also be associated with EVs [29]. The observed four-fold increase in COPD samples compared to healthy controls may suggest a higher amount of lipoproteins in the BALF of COPD patients or a higher capacity of COPD EVs to bind lipoproteins. Studies in sputum from patients with mild COPD revealed lower ApoA1 expression compared to smokers without lung pathology [30]. In contrast, overexpression of ApoA1 in the alveolar epithelium protected mice from developing cigarette-smoke-induced emphysema [31]. These conflicting findings highlight the uncertainty surrounding the precise role of ApoA1 in the pathogenesis of COPD.

The most down-regulated protein observed in COPD BALF EVs was GPM6A. Interestingly, prior reports have highlighted its secretion in EVs, a process influenced by stressors in the blood [32]. Additionally, GPM6A is possibly involved in Alzheimer's disease [33]. According to the human protein atlas [34], GPM6A is primarily expressed in the alveolar epithelium. This particular location makes this a compelling protein to investigate in the context of COPD. Despite its secretion in EVs under stress conditions, and its association with Alzheimer's disease, there is currently no documented report specifically linking GPM6A to human lungs or pulmonary EVs.

The top up-regulated EV-associated miRNAs—miR-122-5p, miR-449c-5p, miR-10a-5p and miR-155-5p—reveal intriguing connections within the context of COPD. Starting with miR-122-5p, it has been found to be downregulated in lung tissue-derived EVs of COPD patients in comparison to healthy smokers [35]. Further studies demonstrated its downregulation in sputum and plasma of COPD patients during exacerbation, indicating its role as a negative regulator of IL-17A production [36]. In plasma-derived EVs from patients with asthma, miR-122-5p was increased [10]. These contrasting effects in different compartments and diseases suggest that miRNA expression might depend on specific cell type activation within a particular context. Regarding the up-regulation of miR-449c-5p, our results align with a study in COPD demonstrating a higher expression of this miRNA in BAL-derived extracellular miRNAs of COPD patients compared to smokers and non-smokers [37]. Similarly, miR-10a-5p was found to be higher in bronchial epithelial cells from patients with asthma and COPD compared to controls [38]. Studies on miR-155-5p showed higher expression in the lung tissue of smokers without airflow limitation and patients with COPD compared to never-smokers, and its inhibition in mice demonstrated an attenuated CS-induced pulmonary inflammation, suggesting a role in COPD pathogenesis [39]. In our study, we observed increased miR-155 in BALF EV of COPD patients. This heightened expression, combined with the inflammatory proteins associated with EVs, could potentially contribute to the perpetuation of pulmonary inflammation in COPD.

We found some interesting correlations within the presence of specific proteins in BALF. In controls, both LGALS3BP and BAIAP2L1 correlated negatively with BALF macrophage numbers. LGALS3BP is a ubiquitously expressed cellular secreted glycoprotein with multiple antiviral activities. Its expression is stimulated by IFNs, resulting in upregulated 90 K serum concentrations in individuals with viral infections [40]. The negative association

with macrophage numbers in controls could relate to the absence of infections in these healthy individuals.

In COPD EVs, AQP1 showed a positive correlation with macrophage numbers. AQP1 functions as a water channel, fostering migration in various cell types [41]. However, in macrophages, the impact of AQP1-induced migration depends on external stimuli. In a model of acute bacterial peritonitis, mice lacking AQP1 (Aqp1<sup>-/-</sup>) displayed reduced infiltrating M1 macrophages when exposed to LPS stimulation [42]. Additionally, resting Aqp1<sup>-/-</sup> macrophages shifted from M0 to an M2 phenotype. This means that the observed correlation of AQP1 with macrophage numbers in COPD might signify a higher presence of activated M1 macrophages.

With regard to lung function, specific proteins within EVs showed correlations with the FEV1/FVC parameter. In control EVs, abundance of Lipocalin-2 (LCN2) correlated positively to FEV1/FVC ( $r = 0.60$ ,  $p = 0.03$ ). This holds significance as LCN2 is known for its vital roles in airway defense, particularly in attenuating inflammation and aiding pathogen clearance [43]. Conversely, in COPD EVs, more LTF correlated with lower FEV1/FVC ( $r = -0.50$ ,  $p = 0.04$ ). This aligns with a recent study in a mouse model of particulate matter (PM)-induced pulmonary injury, where more LTF protein was found in PM-exposed lung tissues, indicating LTF's possible involvement in lung injury triggered by PM exposure [44].

We realize that there are some limitations of our current study. The use of samples stored at  $-80$  degrees Celsius for over 20 years [9] might have impacted sample quality. Although, since all samples were consistently handled and never thawed before this study, we are confident that these valuable samples can still be used to generate hypotheses regarding the role that EVs in the COPD lung pathology. Furthermore, we successfully identified a substantial number of proteins, including several classical EV markers, and achieved a sufficient sequencing depth of 1 million reads for miRNAs. The integrity of the EVs following the extended storage duration was confirmed through cryo-TEM. Regarding EV isolations containing lipoproteins, this occurrence was expected due to the method employed, specifically SEC, which does not effectively separate lipoproteins from small EVs [20]. Given the limited material and the complexity of employing multiple isolation techniques, complete separation would have been technically unfeasible [45]. Recognizing the presence of lipoproteins alongside EVs is important for future interpretations.

Additionally, the utilization of *in silico* tools like IPA analysis and FunRich software (Version 3.1.4) provides an initial framework for insight and hypothesis generation based on established associations in the literature. However, it is important to acknowledge that these findings would benefit from confirmation through mechanistic experiments in future studies to validate and enhance their significance. Our cluster analysis confirmed the abundant presence of proteins linked to immune activation pathways. Furthermore, the correlations observed between the abundance of some of these proteins with macrophage numbers and lung function represent compelling points of interest. These correlations suggest potential links between specific proteins, immune response pathways, and clinical parameters, offering valuable insights into the complex interplay within COPD pathophysiology.

Our proteomics analysis identified more unique protein IDs in the COPD BALF EVs as compared to the control EVs. This disparity could arise from either a higher protein content of COPD EVs, or an increased quantity of EVs in BALF samples of patients with COPD. Although the NTA did not directly measure the EV count, the elevated expression intensity of classical EV markers, as defined by the MISEV2018 guidelines [19], might support the latter hypothesis. However, quantifying EVs using common markers such as tetraspanins might not be accurate, as their expression can significantly vary based on EV source and external stimuli [46]. Furthermore, evidence suggests that EVs can carry a protein corona on their surface, consisting of proteins like ApoA1, ApoB, ApoE, complement factors 3 and 4B, fibrinogen  $\alpha$ -chain, immunoglobulin heavy constant  $\gamma$ 2 and  $\gamma$ 4 chains, many of which are found to be increased in our dataset [29]. Interestingly, studies demonstrated that EVs bearing a corona induce a stronger inflammatory response in human monocyte-derived dendritic cells compared to EV-free protein aggregates [29]. It

is thus very intriguing to speculate that EVs in the BALF also carry such a protein corona, which might be functionally involved in COPD pathogenesis.

In our study, there was a disparity in smoking status between the two groups. Due to the small sample size and the predominance of ex-smokers, we did not control for smoking. However, we conducted a correlation analysis on significant protein abundances comparing all samples, with and without the three non-smoking COPD patients. As depicted in Figure S2, this analysis demonstrated a high degree of correlation, indicating that the inclusion of non-smoking patients did not significantly impact our findings. Moreover, it is plausible that these non-smoking patients may have been exposed to passive or even third-hand smoke from a smoking partner or at the workplace. This can no longer be verified.

## 5. Summary and Conclusions

This is the first study to investigate both the protein and small RNA content of EVs derived from BALF samples from patients with COPD and healthy controls. We show here that good quality EVs can be isolated from BALF samples that have been stored at  $-80^{\circ}\text{C}$  for an extended period of time. We also showed that the protein content of EVs is significantly altered in COPD and has an association with increased inflammatory responses and cellular damage in the lungs. BALF creates a unique opportunity to study the effects of EVs on the pathogenesis of COPD, given that the lower complexity of the biological fluid in this compartment and the identified targets of this study may already provide a good starting point for further targeting. Furthermore, vesicles are received directly from the disease microenvironment and may appear earlier in BALF than in peripheral circulation. More research is needed to decipher the complex role of EV-associated molecules in COPD pathogenesis, which could potentially also reveal novel therapeutic candidates.

**Supplementary Materials:** The following supporting information can be downloaded at: <https://www.mdpi.com/article/10.3390/cells13110945/s1>, Figure S1: Images of COPD-EVs using cryo-TEM. Figure S2: Correlation analysis on significant protein abundances comparing all samples with and without non-smoking COPD patients. Table S1: Complete list of detected proteins in >70% of all samples; Table S2: Receptors on BALF EVs; Table S3: Ligands on BALF EVs; Table S4: List of detected miRNAs in BALF EVs.

**Author Contributions:** Conceptualization, S.B., J.C.W., M.v.d.B. and M.N.H.; methodology, S.B., J.C.W., E.N.-'t.H., K.R., J.F. and M.W.P.; software, S.B., H.N. and B.K.; validation, J.C.W., M.W.P., K.R., J.F. and M.N.H.; formal analysis, S.B., J.C.W., H.N. and B.K.; patient material resources, S.R., W.T. and M.v.d.B.; data curation, S.B., H.N. and M.N.H.; writing—original draft preparation, S.B. and H.N.; writing—review and editing, S.B., J.C.W., H.N., B.K., E.N.-'t.H., M.W.P., K.R., J.F., S.R., W.T., M.v.d.B. and M.N.H.; supervision, M.N.H.; project administration, M.N.H.; funding acquisition, S.B. and M.N.H. All authors have read and agreed to the published version of the manuscript.

**Funding:** This research was funded by a Longfonds Junior Investigator Grant to S.B. (Project 4.2.19.040JO), the Stichting Astma Bestrijding (SAB, Project 2021-021) and the Noordelijke Cara Stichting (NCS, Project 2019/02).

**Institutional Review Board Statement:** Ethical review and approval was waived for this study because the study was conducted so long ago that we no longer sought permission for the EV-related portion of this study.

**Informed Consent Statement:** Patient consent was waived because the study was conducted already more than 25 years ago.

**Data Availability Statement:** The mass spectrometry proteomics data have been deposited to the ProteomeXchange Consortium via the PRIDE [47] partner repository with the dataset identifier PXD049998.

**Acknowledgments:** We would like to thank Wierd Kooistra and Marjan Reinders-Luinge for the excellent technical assistance.

**Conflicts of Interest:** The authors declare no conflicts of interest.



## References

1. Cosio, M.G.; Saetta, M.; Agusti, A. Immunologic Aspects of Chronic Obstructive Pulmonary Disease. *N. Engl. J. Med.* **2009**, *360*, 2445–2454. [CrossRef]
2. Sundar, I.K.; Li, D.; Rahman, I. Small RNA-sequence analysis of plasma-derived extracellular vesicle miRNAs in smokers and patients with chronic obstructive pulmonary disease as circulating biomarkers. *J. Extracell. Vesicles* **2019**, *8*, 1684816. [CrossRef]
3. Raposo, G.; Stoorvogel, W. Extracellular vesicles: Exosomes, microvesicles, and friends. *J. Cell Biol.* **2013**, *200*, 373–383. [CrossRef]
4. Mittelbrunn, M.; Gutiérrez-Vázquez, C.; Villarroya-Beltri, C.; González, S.; Sánchez-Cabo, F.; González, M.Á.; Bernad, A.; Sánchez-Madrid, F. Unidirectional transfer of microRNA-loaded exosomes from T cells to antigen-presenting cells. *Nat. Commun.* **2011**, *2*, 282. [CrossRef]
5. French, K.C.; Antonyak, M.A.; Cerione, R.A. Extracellular vesicle docking at the cellular port: Extracellular vesicle binding and uptake. *Semin. Cell Dev. Biol.* **2017**, *67*, 48–55. [CrossRef]
6. Bartel, S.; Deshane, J.; Wilkinson, T.; Gabrielsson, S. Extracellular Vesicles as Mediators of Cellular Cross Talk in the Lung Microenvironment. *Front. Med.* **2020**, *7*, 326. [CrossRef]
7. Genschmer, K.R.; Russell, D.W.; Lal, C.; Szul, T.; Bratcher, P.E.; Noerager, B.D.; Abdul Roda, M.; Xu, X.; Rezonzew, G.; Viera, L.; et al. Activated PMN Exosomes: Pathogenic Entities Causing Matrix Destruction and Disease in the Lung. *Cell* **2019**, *176*, 113–126. [CrossRef]
8. Monsel, A.; Zhu, Y.G.; Gudapati, V.; Lim, H.; Lee, J.W. Mesenchymal stem cell derived secretome and extracellular vesicles for acute lung injury and other inflammatory lung diseases. *Expert Opin. Biol. Ther.* **2016**, *16*, 859–871. [CrossRef]
9. Rutgers, S.R.; Timens, W.; Kaufmann, H.F.; van der Mark, T.W.; Köeter, G.H.; Postma, D.S. Comparison of induced sputum with bronchial wash, bronchoalveolar lavage and bronchial biopsies in COPD. *Eur. Respir. J.* **2000**, *15*, 109–115. [CrossRef]
10. Węgrzyn, A.B.; Herzog, K.; Gerding, A.; Kwiatkowski, M.; Wolters, J.C.; Dolga, A.M.; van Lint, A.E.M.; Wanders, R.J.A.; Waterham, H.R.; Bakker, B.M. Fibroblast-specific genome-scale modelling predicts an imbalance in amino acid metabolism in Refsum disease. *FEBS J.* **2020**, *287*, 5096–5113. [CrossRef]
11. Bahmer, T.; Krauss-Etschmann, S.; Buschmann, D.; Behrends, J.; Watz, H.; Kirsten, A.M.; Pedersen, F.; Waschki, B.; Fuchs, O.; Pfaffl, M.W.; et al. RNA-seq-based profiling of extracellular vesicles in plasma reveals a potential role of miR-122-5p in asthma. *Allergy Eur. J. Allergy Clin. Immunol.* **2021**, *76*, 366–371. [CrossRef]
12. Akhmedov, M.; Martinelli, A.; Geiger, R.; Kwee, I. Omics Playground: A comprehensive self-service platform for visualization, analytics and exploration of Big Omics Data. *NAR Genom. Bioinform.* **2020**, *2*, lqz019. [CrossRef] [PubMed]
13. Kong, Y. Btrim: A fast, lightweight adapter and quality trimming program for next-generation sequencing technologies. *Genomics* **2011**, *98*, 152–153. [CrossRef] [PubMed]
14. RNAcentral Consortium. RNAcentral 2021: Secondary structure integration, improved sequence search and new member databases. *Nucleic Acids Res.* **2021**, *8*, D212–D220. [CrossRef]
15. Kozomara, A.; Griffiths-Jones, S. MiRBase: Annotating high confidence microRNAs using deep sequencing data. *Nucleic Acids Res.* **2014**, *42*, D68–D73. [CrossRef] [PubMed]
16. Langmead, B.; Trapnell, C.; Pop, M.; Salzberg, S.L. Ultrafast and memory-efficient alignment of short DNA sequences to the human genome. *Genome Biol.* **2009**, *10*, R25. [CrossRef]
17. Love, M.I.; Huber, W.; Anders, S. Moderated estimation of fold change and dispersion for RNA-seq data with DESeq2. *Genome Biol.* **2014**, *15*, 550. [CrossRef]
18. R Development Core Team. *R: A Language and Environment for Statistical Computing*; R Foundation for Statistical Computing: Vienna, Austria, 2011; Available online: <http://www.R-project.org/> (accessed on 5 September 2021).
19. Théry, C.; Witwer, K.W.; Aikawa, E.; Alcaraz, M.J.; Anderson, J.D.; Andriantsitohaina, R.; Antoniou, A.; Arab, T.; Archer, F.; Atkin-Smith, G.K.; et al. Minimal information for studies of extracellular vesicles 2018 (MISEV2018): A position statement of the International Society for Extracellular Vesicles and update of the MISEV2014 guidelines. *J. Extracell. Vesicles* **2018**, *7*, 1535750. [CrossRef]
20. Stam, J.; Bartel, S.; Bischoff, R.; Wolters, J.C. Isolation of extracellular vesicles with combined enrichment methods. *J. Chromatogr. B Anal. Technol. Biomed. Life Sci.* **2021**, *1169*, 122604. [CrossRef]
21. Shao, X.; Liao, J.; Li, C.; Lu, X.; Cheng, J.; Fan, X. CellTalkDB: A manually curated database of ligand–receptor interactions in humans and mice. *Brief. Bioinform.* **2021**, *22*, bbaa269. [CrossRef]
22. Pathan, M.; Keerthikumar, S.; Ang, C.S.; Gangoda, L.; Quek, C.Y.; Williamson, N.A.; Mouradov, D.; Sieber, O.M.; Simpson, R.J.; Salim, A.; et al. FunRich: An open access standalone functional enrichment and interaction network analysis tool. *Proteomics* **2015**, *15*, 2597–2601. [CrossRef] [PubMed]
23. Dubin, R.F.; Robinson, S.K.; Widdicombe, J.H. Secretion of lactoferrin and lysozyme by cultures of human airway epithelium. *Am. J. Physiol.-Lung Cell. Mol. Physiol.* **2004**, *286*, L750–L755. [CrossRef]
24. Thompson, A.B.; Bohling, T.; Payvandi, F.; Rennard, S.I. Lower respiratory tract lactoferrin and lysozyme arise primarily in the airways and are elevated in association with chronic bronchitis. *J. Lab. Clin. Med.* **1990**, *115*, 148–158.

25. Pierce, L.M.; Kurata, W.E. Priming With Toll-Like Receptor 3 Agonist Poly(I:C) Enhances Content of Innate Immune Defense Proteins but Not MicroRNAs in Human Mesenchymal Stem Cell-Derived Extracellular Vesicles. *Front. Cell Dev. Biol.* **2021**, *9*, 676356. [[CrossRef](#)]
26. Müller, H.; Schmiedl, A.; Weiss, C.; Ai, M.; Jung, S.; Renner, M. DMBT1 is upregulated in lung epithelial cells after hypoxia and changes surfactant ultrastructure. *Pediatr. Pulmonol.* **2020**, *55*, 2964–2969. [[CrossRef](#)]
27. Müller, H.; Nagel, C.; Weiss, C.; Mollenhauer, J.; Poeschl, J. Deleted in malignant brain tumors 1 (DMBT1) elicits increased VEGF and decreased IL-6 production in type II lung epithelial cells. *BMC Pulm. Med.* **2015**, *15*, 32. [[CrossRef](#)] [[PubMed](#)]
28. Chen, C.Y.; Rao, S.S.; Ren, L.; Hu, X.K.; Tan, Y.J.; Hu, Y.; Luo, J.; Liu, Y.W.; Yin, H.; Huang, J.; et al. Exosomal DMBT1 from human urine-derived stem cells facilitates diabetic wound repair by promoting angiogenesis. *Theranostics* **2018**, *8*, 1607–1623. [[CrossRef](#)] [[PubMed](#)]
29. Tóth, E.Á.; Turiák, L.; Visnovitz, T.; Cserép, C.; Mázló, A.; Sódar, B.W.; Försönits, A.I.; Petővári, G.; Sebestyén, A.; Komlósi, Z.; et al. Formation of a protein corona on the surface of extracellular vesicles in blood plasma. *J. Extracell. Vesicles* **2021**, *10*, e12140. [[CrossRef](#)] [[PubMed](#)]
30. Titz, B.; Sewer, A.; Schneider, T.; Elamin, A.; Martin, F.; Dijon, S.; Luettich, K.; Guedj, E.; Vuillaume, G.; Ivanov, N.V.; et al. Alterations in the sputum proteome and transcriptome in smokers and early-stage COPD subjects. *J. Proteom.* **2015**, *128*, 306–320. [[CrossRef](#)]
31. Kim, C.; Lee, J.M.; Park, S.W.; Kim, K.S.; Lee, M.W.; Paik, S.; Jang, A.S.; Kim, D.J.; Uh, S.; Kim, Y.; et al. Attenuation of cigarette smoke-induced emphysema in mice by apolipoprotein A-1 overexpression. *Am. J. Respir. Cell Mol. Biol.* **2016**, *54*, 91–102. [[CrossRef](#)]
32. Monteleone, M.C.; Billi, S.C.; Brocco, M.A.; Frasc, A.C. Neural glycoprotein M6a is released in extracellular vesicles and modulated by chronic stressors in blood. *Sci. Rep.* **2017**, *7*, 9788. [[CrossRef](#)] [[PubMed](#)]
33. Muraoka, S.; DeLeo, A.M.; Sethi, M.K.; Yukawa-Takamatsu, K.; Yang, Z.; Ko, J.; Hogan, J.D.; Ruan, Z.; You, Y.; Wang, Y.; et al. Proteomic and biological profiling of extracellular vesicles from Alzheimer’s disease human brain tissues. *Alzheimer’s Dement.* **2020**, *16*, 896–907. [[CrossRef](#)] [[PubMed](#)]
34. The Human Protein Atlas [Internet]. Available online: <https://www.proteinatlas.org/> (accessed on 4 November 2021).
35. Kaur, G.; Maremanda, K.P.; Campos, M.; Chand, H.S.; Li, F.; Hirani, N.; Haseeb, M.A.; Li, D.; Rahman, I. Distinct exosomal miRNA profiles from balf and lung tissue of copd and ipf patients. *Int. J. Mol. Sci.* **2021**, *22*, 11830. [[CrossRef](#)] [[PubMed](#)]
36. Zhu, K.; Zhou, S.; Xu, A.; Sun, L.; Li, M.; Jiang, H.; Zhang, B.; Zeng, D.; Fei, G.; Wang, R. Microbiota Imbalance Contributes to COPD Deterioration by Enhancing IL-17a Production via miR-122 and miR-30a. *Mol. Ther.-Nucleic Acids* **2020**, *22*, 520–529. [[CrossRef](#)] [[PubMed](#)]
37. Cerón-Pisa, N.; Iglesias, A.; Shafiek, H.; Martín-Medina, A.; Esteva-Socias, M.; Muncunill, J.; Fleischer, A.; Verdú, J.; Cosío, B.G.; Sauleda, J. Hsa-Mir-320c, Hsa-Mir-200c-3p, and Hsa-Mir-449c-5p as Potential Specific miRNA Biomarkers of COPD: A Pilot Study. *Pathophysiology* **2022**, *29*, 143–156. [[CrossRef](#)] [[PubMed](#)]
38. Tsai, M.J.; Tsai, Y.C.; Chang, W.A.; Lin, Y.S.; Tsai, P.H.; Sheu, C.C.; Kuo, P.L.; Hsu, Y.L. Deducting microRNA-mediated changes common in bronchial epithelial cells of asthma and chronic obstructive pulmonary disease—A next-generation sequencing-guided bioinformatic approach. *Int. J. Mol. Sci.* **2019**, *20*, 553. [[CrossRef](#)] [[PubMed](#)]
39. De Smet, E.G.; Van Eeckhoutte, H.P.; Avila Cobos, F.; Blomme, E.; Verhamme, F.M.; Provoost, S.; Verleden, S.E.; Venken, K.; Maes, T.; Joos, G.F.; et al. The role of miR-155 in cigarette smoke-induced pulmonary inflammation and COPD. *Mucosal Immunol.* **2020**, *13*, 423–436. [[CrossRef](#)]
40. Xu, G.; Xia, Z.; Deng, F.; Liu, L.; Wang, Q.; Yu, Y.; Wang, F.; Zhu, C.; Liu, W.; Cheng, Z.; et al. Inducible LGALS3BP/90K activates antiviral innate immune responses by targeting TRAF6 and TRAF3 complex. *PLoS Pathog.* **2019**, *15*, e1008002. [[CrossRef](#)] [[PubMed](#)]
41. Quan, Y.; Kan, B.; Yang, B. Aquaporins in Immune System. *Adv. Exp. Med. Biol.* **2023**, *398*, 195–202. [[CrossRef](#)]
42. Tyteca, D.; Nishino, T.; Debaix, H.; Van Der Smissen, P.; N’Kuli, F.; Hoffmann, D.; Cnops, Y.; Rabolli, V.; van Loo, G.; Beyaert, R.; et al. Regulation of macrophage motility by the water channel aquaporin-1: Crucial role of M0/M2 phenotype switch. *PLoS ONE* **2015**, *26*, e0117398. [[CrossRef](#)]
43. Chan, Y.R.; Liu, J.S.; Pociask, D.A.; Zheng, M.; Mietzner, T.A.; Berger, T.; Mak, T.W.; Clifton, M.C.; Strong, R.K.; Ray, P.; et al. Lipocalin 2 is required for pulmonary host defense against Klebsiella infection. *J. Immunol.* **2009**, *182*, 4947–4956. [[CrossRef](#)] [[PubMed](#)]
44. Yan, L.; Chen, S.; Hou, C.; Lin, J.; Xiong, W.; Shen, Y.; Zhou, T. Multi-omics analysis unravels dysregulated lysosomal function and lipid metabolism involved in sub-chronic particulate matter-induced pulmonary injury. *Sci. Total Environ.* **2022**, *836*, 155642. [[CrossRef](#)] [[PubMed](#)]
45. Dong, L.; Zieren, R.C.; Horie, K.; Kim, C.J.; Mallick, E.; Jing, Y.; Feng, M.; Kuczler, M.D.; Green, J.; Amend, S.R.; et al. Comprehensive evaluation of methods for small extracellular vesicles separation from human plasma, urine and cell culture medium. *J. Extracell. Vesicles* **2020**, *10*, e12044. [[CrossRef](#)] [[PubMed](#)]



46. Mizenko, R.R.; Brostoff, T.; Rojalin, T.; Koster, H.J.; Swindell, H.S.; Leiserowitz, G.S.; Wang, A.; Carney, R.P. Tetraspanins are unevenly distributed across single extracellular vesicles and bias sensitivity to multiplexed cancer biomarkers. *J. Nanobiotechnol.* **2021**, *19*, 250. [[CrossRef](#)] [[PubMed](#)]
47. Perez-Riverol, Y.; Bai, J.; Bandla, C.; Hewapathirana, S.; García-Seisdedos, D.; Kamatchinathan, S.; Kundu, D.; Prakash, A.; Frericks-Zipper, A.; Eisenacher, M.; et al. The PRIDE database resources in 2022: A Hub for mass spectrometry-based proteomics evidences. *Nucleic Acids Res.* **2022**, *50*, D543–D552. [[CrossRef](#)]

**Disclaimer/Publisher’s Note:** The statements, opinions and data contained in all publications are solely those of the individual author(s) and contributor(s) and not of MDPI and/or the editor(s). MDPI and/or the editor(s) disclaim responsibility for any injury to people or property resulting from any ideas, methods, instructions or products referred to in the content.